ULTRAFAST LASER TEXTURING OF TI-6AL-4V SURFACES FOR BIOMEDICAL APPLICATIONS

Paper Number: **#N405**

Alexandre Cunha[1,2,6], Vitor Oliveira[1,3], Ana Paula Serro[4,5], Omar El-Farouk Zouani[6], Amélia Almeida[1,2], Marie-Christine Durrieu[6], Rui Vilar[1,2]

[1]ICEMS-Instituto de Ciência e Engenharia de Materiais e Superfícies, Av. Rovisco Pais, Lisbon, 1049-001, Portugal
[2]Instituto Superior Técnico-Technical University of Lisbon, Av. Rovisco Pais, Lisbon, 1049-001, Portugal
[3]Instituto Superior de Engenharia de Lisboa, Rua Conselheiro Emídio Navarro, Lisbon, 1959-007, Portugal
[4]Instituto Superior Técnico, Structural Chemistry Centre, Av. Rovisco Pais, Lisbon, 1049-001, Portugal
[5]Instituto Superior de Ciências da Saúde Egas Moniz, Centro de Investigação Interdisciplinar Egas Moniz, Caparica, 2829-511, Portugal
[6] Chimie et Biologie des Membranes et des Nanoobjets (CBMN UMR-CNRS 5248), IECB-Institut Européen de Chimie et Biologie, Université de Bordeaux I, 2 Rue Robert Escarpit, Pessac, 33607, France

Abstract

By controlling processing parameters such as the average fluence, number of laser pulses and beam polarization direction, different types of multiscale surface textures were produced on Ti-6Al-4V surfaces by ultrafast laser processing. The samples were textured in ambient atmosphere using an Yb: KYW chirped-pulse-regenerative amplification laser with a wavelength of 1030 nm and pulse duration of 500 fs. The wetting of simulated biological fluids as well as the human mesenchymal stem cells (hMSCs) behavior were assessed. Three types of textured surfaces were tested, consisting of: (i) Laser-Induced Periodic Surface Structures-LIPSS; (ii) nanopillars-like structures; and (iii) LIPSS overlapped to microcolumns. The laser textured surfaces present hydrophilic behavior and high affinity for HBSS (Hank's balanced salt solution). Cell spreading and adhesion strength is reduced by the laser nanotextures as compared to a polished control surface. Cytoskeleton stretching and stress fibers were clearly observed on LIPSS while significant filopodia formation was verified on nanopillars. There was no cell proliferation on the laser nanotextured surfaces. Ultrafast laser texturing of Ti-6Al-4V surfaces is an efficient technique for increasing surface wettability, and is potentially useful as a technique to control the behavior of hMSCs by changing the cytoskeleton shape, FAPs distribution and area, and proliferation.

Introduction

Mesenchymal stem cells (MSCs) possess a unique characteristic that distinguish them from other types of cells. They are undifferentiated cells that may develop into different cell lineages responsible for the formation of specific tissues such as bone, cartilage, fat, muscle and neurons **[1]**. Due to this unique characteristic, MSCs have become the focus of regenerative medicine and tissue engineering research. Combinations of physical, chemical, and biological cues present in the MSCs microenvironment have been implicated as directors of their *in vivo* fate **[2]**. Implants may make use of topographical and chemical surface modifications to control cell adhesion, differentiation, and de novo tissue formation **[3]**. The surface topography and chemical composition are key factors in controlling implant surface wettability, which directly affects cellular behaviour **[4-5]**. *In vitro* studies indicate that endogenous proteins are rapidly adsorbed at materials surfaces, providing a chemical framework on which cellular adhesion may initiate. Once cells establish their focal adhesion points (FAPs), a series of mechanical and biochemical stimuli trigger a cascade of signals that lead to a modulation in the gene expression, dictating the cell fate **[4]**. The possibility of changing MSCs behavior by simply altering biomaterial surface topography and chemistry justifies the efforts developed in creating surfaces

capable of controlling cell behavior in a reproducible way **[6-10]**. In the past few years, many surface modification techniques such as polymer demixing, imprinting, electron beam lithography and photolithography have been applied in order to produce multiscaled surfaces with different degrees of anisotropy **[11-14]**. However these techniques are usually complex and involve many steps for producing the desired patterned surface. Furthermore, usually the surface pattern can only be created on flat surfaces and model materials, such as polymers. On the contrary, ultrafast laser surface texturing allows creating a wide range of nano- and micro-scaled structures on nearly all types of materials (metals, semiconductors, polymers and ceramics) **[15]**. The process presents unique characteristics such as flexibility, simplicity, controllability and high reproducibility and it may also be applied to the tailoring of real biomaterials surfaces, such as titanium alloys, which are widely used in dental and orthopedic implants.

In previous papers it has been demonstrated that a range of surface textures can be produced on titanium alloys by femtosecond laser processing **[16-17]** and the effect of these textures on wettability studied **[18]**. In the present paper these results are summarily reviewed and the impact of Ti-6Al-4V surface texturing on hMSCs behavior described.

Materials and Methods

Laser Surface Texturing

The experiments were performed on 1.2 mm thick specimens of biomedical grade 5 Ti–6Al–4V alloy with areas of 1.0 x 1.0 and 1.5 x1.0 cm^2. Prior to the laser treatment the specimens were ground with a 320–2400 grit sequence of SiC papers, followed by metallographic polishing with 6 and 3 μm alumina suspensions in water. After polishing, the samples were ultrasonically cleaned for 10 min first in a detergent solution then in acetone for degreasing and removing polishing residues. An Yb: KYW chirped-pulse regenerative amplification laser system (Amplitude Systèmes s-Pulse HP) with a central wavelength of 1030 nm and a laser pulse duration of 500 fs was used for the surface texturing. The laser beam was focused by a 100 mm focal length lens and incident perpendicularly to the sample surface. The direction of its polarization vector in relation to the laser beam scanning direction was controlled by a half-wave plate (λ/2). The average pulse energy was varied in the range 75-705 μJ by means of an attenuator in order to achieve average fluences at the surface of the sample ranging from 0.2 to 0.6 J/cm^2 at pulse repetition rates in the range 1-50 Hz. Laser surface texturing was performed by moving the samples under the stationary laser beam by a computer-controlled XYZ stage with scanning speeds in the range 0.01-0.8 mm/s. To achieve surface coverage a lateral displacement of the laser beam was applied by moving the stage in a direction perpendicular to the laser beam scanning direction. Lateral displacements in the range 90-200 μm were applied in order to partially overlap the linear tracks.

Surface Characterization

The surface topography was observed in secondary electrons imaging mode using a JEOL JSM-7001F field emission gun scanning electron microscope. Three-dimensional plots of the surfaces were created from stereoscopic pairs of SEM images acquired at tilting angles of 0 and 10º using Alicona-MeX© software. The surface roughness was measured according to ISO 4287 standard using a Rodenstock RM 600 non-contact optical profilometer. The roughness was characterized by the arithmetic mean surface roughness (R_a) calculated from the surface profiles. The value of R_a is the average of at least five measurements taken in different regions in directions parallel and perpendicular to the laser beam scanning direction.

Wettability Measurements

Wettability was evaluated by the sessile drop method. The measurements were performed at room temperature using as testing media distilled-deionized (DD) water and Hank's balanced salt solution (HBSS), which simulate the biological fluids. Prior to the measurements the samples were ultrasonically cleaned first with a detergent solution (Extran®), twice in DD water, ethanol and finally in DD water. The duration of sonication in each product was 10 min. After cleaning the remaining water was removed with a nitrogen gas jet and the samples dried in vacuum at room temperature overnight. Droplets of about 4 μL of the testing media were deposited with a micrometric syringe on the samples surface in a closed chamber saturated with water and the contact angle measured by means of a video microscope. The measurements were performed at regular time lapses, starting at the droplet deposition instant until the droplets spreading cessed or at least for 600 s. The droplet profile was analysed using the axisymmetric drop shape analysis profile method (ADSA-P) **[19]**. The static contact angle was estimated by fitting the Laplace equation to the experimental profiles. The values presented are the average of at least five measurements at different locations.

Cell culture

The specimens were ultrasonically cleaned in absolute ethanol during 15 minutes, put on 12-well cell culture plates, washed with 70 % ethanol during 10 minutes and rinsed twice with phosphate buffered saline (PBS). Human Mesenchymal Stem Cells (hMSCs, purchased from Lonza) obtained from bone marrow (STRO-1 selected skeletal stem cells) were allowed to proliferate in plastic T-tubes supplemented with a Gibco alpha minimal essential medium (MEM) containing L-glutamine, ribonucleosides, deoxyribonucleosides, ascorbic acid, 10 % of fetal bovine serum (FBS) and 1 % of penicillin/streptomycin antibiotics. Confluence of the cells was verified by optical microscopy. The MEM was removed from the plastic T-tubes and trypsinization was performed during 5 minutes for cell detachment. The culture medium was then added to the T-tubes and the cells containing solution collected. Cells were seeded on the specimens by adding 2.0 ml of the culture medium on each well-plate. The plates were incubated under controlled atmosphere of 5 % CO_2 at 37 °C. The culture medium was replaced at every two days.

Immunofluorescence

Cell adhesion and spreading analyses were performed 24 h after incubation. The culture medium was removed from the well-plates and cells were fixed with 4 % paraformaldehyde (PFA) in PBS during 30 minutes at a temperature of 4 °C. The specimens were washed twice with PBS and cells permeabilization performed with 0.5 % triton-X-100 diluted in deionized water during 30 minutes at a temperature of 4 °C. The specimens were washed with 1 % bovine serum albumin (BSA) in PBS for 30 minutes at a temperature of 37 °C. Immunofluorescent staining of vinculin was performed with monoclonal anti-vinculin clone hVIN-1 antibody produced in mouse and Alexafluor 568 fragment of rabbit anti-mouse. F-actin fibers filaments were stained with Alexafluor 488-phalloidin. Cell nuclei were stained with a gold antifade reagent with DAPI (4, 6-diamidino-2-phenylindole). Incubation of the anti-vinculin (1:200) in 1 % BSA/PBS was performed for 1 h at 37 °C. The secondary antibody Alexafluor 568 (1:200) in 1 % BSA/PBS was incubated during 30 minutes at room temperature. Alexafluor 488-phalloidin (1:40) in 1 % BSA/PBS was incubated for 1 h at 37 °C. After each incubation step the specimens were washed twice in 0.05 % Tween 20 (polyoxyrthylenesorbitan monolaurate) in PBS. Finally, the culture substrates were mounted on glass microscope slides and incubated with DAPI by adding one droplet to each one. Cytoskeleton organization and cell proliferation analyses were performed at 2 weeks after incubation. Immunofluorescent staining for F-actin fibers filaments and cell nucleus was performed with Alexafluor 488-phalloidin and a gold antifade reagent with DAPI, as previously described. Fluorescent micrographs were taken with a LEICA CTR 6000 fluorescence microscope with three different wavelengths: 358 nm (blue), 488 nm (green) and 568 nm (red). Cells were stained green for F-actin fibers filaments, blue for nucleus, and red for vinculin. At least 10 images of each group were taken at different magnifications. FAPs area and cell proliferation analysis was performed by using Image J freeware (NIH, http://rsb.info.nih.gov/ij/). The vinculin stained micrographs were used for the measurements of the FAPs area. The DAPI stained micrographs were used for the estimation of the average number of nuclei at the different culture periods by using the cell counting function. Then, cell proliferation (CP) was estimated by using the equation (1):

$$\mathrm{CP}\ (\%) = \frac{N_{2weeks} - N_{24h}}{N_{2weeks}} \mathrm{x}\ 100, \qquad (1)$$

where, N_{24h} *and* N_{2weeks} are the average number of nuclei at 24h and 2 weeks, respectively.

Results

Surface textures

Representative SEM micrographs of the three types of textured surfaces tested are presented in **Figure 1**. These surface textures consist of LIPSS (**Figure 1A-B**, Type 1 texture), an array of nanopillars (**Figure 1C-D**, Type 2 texture), and LIPSS nano-textured microcolumns (**Figure 1E-F**, Type 3 texture), forming a bimodal texture consinsting of LIPSS overlapped onto microcolumns (**Figure 1G**). A fourth type of textured surface (Type 4 texture) was produced by creating a pattern of parallel lines consisting of nano-textured microcolumns. The periodicty of the microgrooves is of about 200 μm. The conditions for producing these textures were described in a previous paper **[18]**. The first type of surface texture consists of periodic waves with an average period $\lambda = 820 \pm 50$ nm. It was obtained with an average fluence of 0.3 J/cm^2 and a scanning speed of 0.2 mm/s, corresponding to 65 laser pulses per

surface point. The LIPSS are oriented perpendicularly to the polarization vector of the linearly polarized laser beam. The surface roughness in a direction perpendicular to the LIPSS is R_a = 290 ± 20 nm.

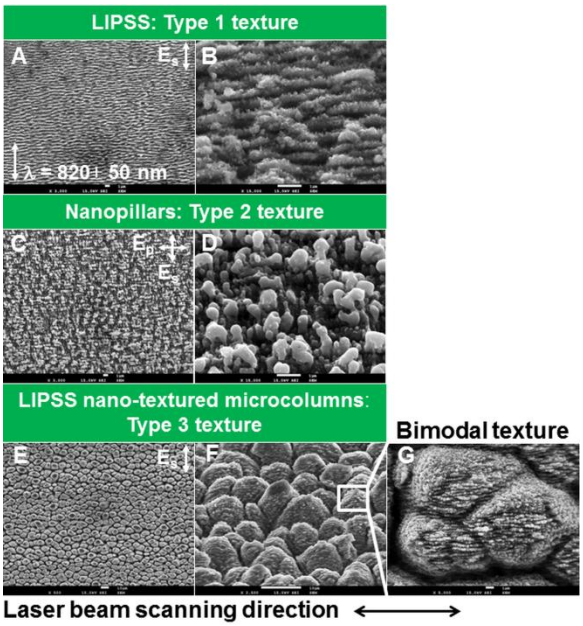

Figure 1. SEM micrographs of the textured surfaces.

Type 2 texture was created by overlaping LIPSS with mutually perpendicular orientations. In the present case the first step was carried out with an average fluence of 0.3 J/cm^2 and a scanning speed of 0.2 mm/s and the second step with an average fluence of 0.2 J/cm^2 and a scanning speed of 0.8 mm/s after introducing in the laser beam path a half-wave plate to rotate the polarization vector direction by 90º. This surface present R_a = 260 ± 10 nm. Type 3 texture was obtained with an average fluence of 0.6 J/cm^2 and a scanning speed of 0.1 mm/s, corresponding to 188 laser pulses per surface point. The mean height of the colums is 4.4 ± 1.3 µm. The surface roughness is R_a = 1.1 ± 0.1 µm. Finally, the fourth type of surface texture (Type 4) is obtained when the surface is treated with an average fluence of 0.6 J/cm^2 and a scanning speed of 0.01 mm/s, corresponding to 1880 laser pulses per surface point. This texture also consists of LIPSS overlapped onto microcolumns but, in contrast with Type 3 texture, it presents periodic ridges aligned in the laser beam scanning direction consisting of large columns with 27.0 ± 15.0 µm mean height separated by wide depressions consisting of columns similar to those found in Type 3 texture. Their periodicity is equal to the lateral displacement of the laser beam to overlap tracks (200 µm). The roughness of this surface is R_a = 4.7 ± 0.6 µm.

Wetting Behavior

The evolution of the contact angle with time for water and HBSS on the smooth and laser textured surfaces is presented in **Figures 2A** and **B**, respectively. The smooth surface presents a time independent hydrophilic behaviour and a high affinity for HBSS. The smooth surface is wetted by both liquids and the contact angles are very similar for the two liquids (68.0 and 63.4º for DD water and HBSS, respectively after 600 s of contact).

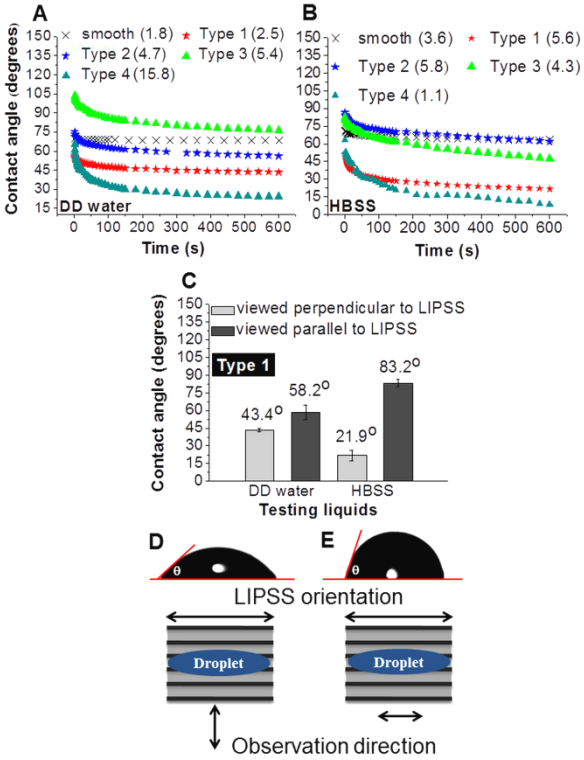

Figure 2. Evolution of the contact angle with time for DD water (A) and HBSS (B) droplets on the smooth control and the laser textured surfaces; anisotropic wetting on Type 1 texture (C-E).

On the contrary, the laser textured surfaces present a time-dependent behaviour. At t = 0 s all surfaces except Type 3 are wetted by water (θ < 90º). HBSS wets all laser textured surfaces including Type 3. The best wetting is achieved for surfaces Type 1 and 4 for both liquids, with equilibrium contact angles of 43.4 and 24.1º for water and 21.9 and 8.4º for HBSS, respectively. The decrease of the contact angle with HBSS is maximum for surfaces with Type 4 texture and after reaching a very low contact angle of about 8.0º the droplets spread over all the treated area, allowing no further measurements. Surfaces with textures Types 2 and 3 present a wetting similar to the smooth control surface, with equilibrium contact

angles of 56.2 and 76.2º for water and 61.8 and 47.6º for HBSS, respectively. The anisotropy of Type 1 texture leads to an anisotropic wetting, since the droplets spread mainly in the LIPSS direction (**Figure 2C**). The equilibrium contact angles are 43.4 and 21.9º for water and HBSS, respectively (**Figure 2C-D**) when the droplets are imaged perpendicularly to the LIPSS and 58.2 and 83.2º when they are observed in a direction parallel to the LIPSS (**Figure 2C and E**). The anisotropy is more important for HBSS than for water ($\Delta\theta$ = 61.3º for HBSS and 14.8º for water). The kinetics of drop spreading for both liquids on the laser textured surfaces was also evaluated, since the wetting is clearly dependent on time as aforementioned. The spreading coefficient is approximately 60% higher for HBSS than for water (0.14 vs 0.08, respectively). Further, the droplets tend to spread faster on the anisotropic textures. A detailed analysis of these results can be found in a previous publication **[18]**.

HMSCs Behavior

Representative fluorescent micrographs of the cells 24 h after incubation are shown in **Figure 3**.

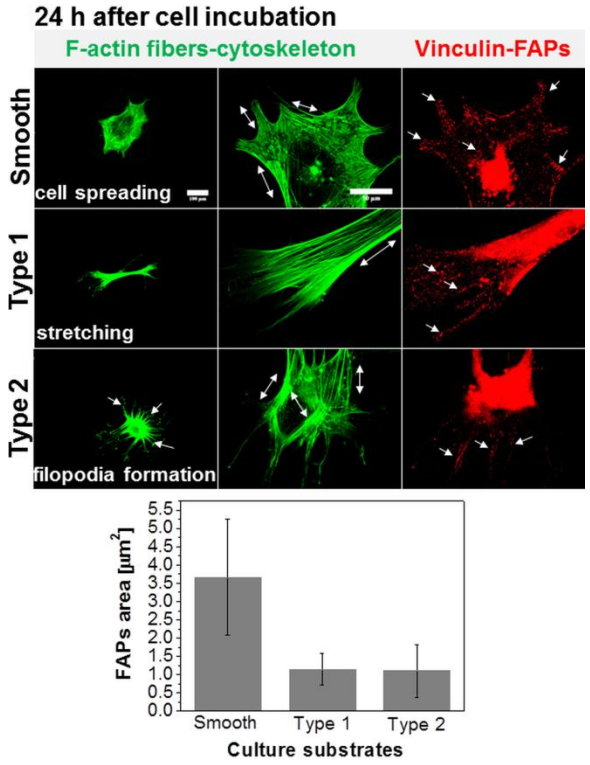

Figure 3. Representative fluorescent micrographs for the smooth control and laser nanotextured surfaces 24 h after cell incubation; F-actin fibers (cytoskeleton) is stained green and vinculin (focal adhesion points-FAPs) in red; F-actin fibers orientation, filopodia and FAPs (white arrows); quantification of FAPs area.

It is clear that hMSCs are sensitive to the surface topography. Different surfaces induce quite distinct arrangements of the cell cytoskeleton (F-actin fibers) as well as distributions and areas of the focal adhesion points (FAPs). Staining of polymerized F-actin fibers reveals that cells cultured on the smooth control surfaces present a significant spreading in comparison with cells cultured on laser nanotextured surfaces. Cell spreading is approximately homogeneous (no preferential alignment of F-actin fibres, white arrows). Cells cultured on LIPSS textured surfaces (Type 1) show preferential cytoskeleton stretching. Stress fibers, where a bundle of polymerized F-actin fibers appear preferentially stretched and aligned in the same stretching direction of the cell cytoskeleton are observed (white arrow). A few cell membrane extensions (filopodia) are visualized at cell extremities. Cells cultured on Type 2 surfaces (nanopillars) do not show preferential cytoskeleton stretching and the F-actin fibers (white arrows) are similar to the control surface. However, an expressive formation of filopodia homogeneously distributed around the cell cytoskeleton is observed. FAPs, revealed by vinculin staining, are observed on all surfaces and present an elongated shape but their distribution and area change significantly for different surfaces.

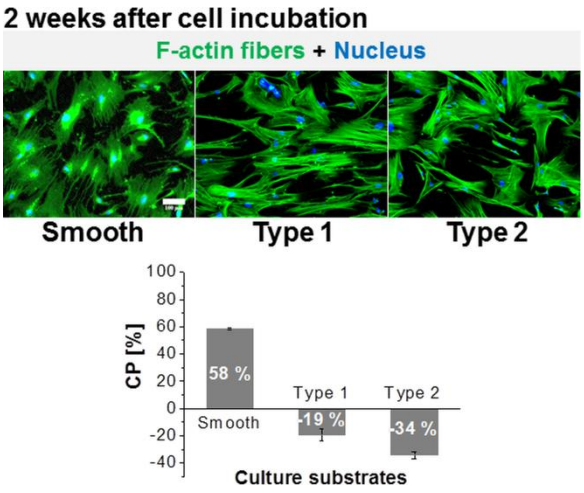

Figure 4. Representative fluorescent micrographs and cell proliferation for the smooth control and laser nanotextured surfaces 2 weeks after cell incubation; F-actin fibers (cytoskeleton) is stained green and nucleus in blue.

For the smooth control surface FAPs are distributed around the cytoskeleton edges (lamellipodia region) and around the nucleus region. Their area is about 3.7

± 1.6 μm^2. For the laser treated surfaces FAPs are concentrated at the cell extremities, mainly at the sites of filopodia structures. Their area decreases to 1.2 ± 0.4 and 1.1 ± 0.7 μm^2 for Type 1 and Type 2 surfaces, respectively. Cytoskeleton organization and cell proliferation 2 weeks after incubation are shown in **Figure 4**. The cytoskeleton organization after 2 weeks is similar to that observed after 24 h. Cells are well spread on the smooth control surfaces, a collective cell alignment is observed on LIPSS, and less filopodia formation is verified in cells cultured on nanopillar textures. Cell proliferation was 58 % on the control surfaces. On the contrary, there was no proliferation for cells in contact with the laser nanotextured surfaces.

Discussion

The present work shows that different surface textures can be produced on Ti-6Al-4V surfaces using ultrafast laser texturing, and that these textures affect the wettability of the material by water and HBSS solution as well as the hMSCs behavior. When the material is treated with average fluences between 0.1–0.3 J/cm^2 its surface is characterized by the presence of ripples perpendicular to the beam polarization direction, usually called LIPSS (Type 1 texture). Taking profit of the possibility of controlling the orientation of LIPSS by rotating the beam polarization, a texture consisting of nanopillars (Type 2 texture) was produced by treating the same area twice with laser beam mutually perpendicular polarizations and parameters suitable to form LIPSS. For larger values of the average fluence (0.4 – 2.0 J/cm^2) ablation is more intense and a columnar microtexture forms (Type 3 and 4 textures). Textures consisting of LIPSS overlapping columns, form as the surface is subjected to decreasing fluences when the sample moves linearly under the stationary laser beam. The surface textures prepared in the present work show different degrees of anisotropy. Type 1 texture is clearly anisotropic due to the orientation of LIPSS. On the contrary, Type 2 texture is isotropic because the anisotropy resulting from the first treatment is destroyed when the LIPSS initially produced are fragmented by the second treatment. Surface texture Type 3 is also approximately isotropic because the cross-section is roughly circular and these microcolumns are randomly distributed over the treated area while Type 4 texture presents a strong anisotropy due to the pattern of microgrooves parallel to the laser beam scanning direction. The laser treated surfaces present R_a values varying between 260 nm and 4.7 μm. Types 1 and 2 textures have similar R_a (290 and 260 nm, respectively) but their wettability are quite different, especially for HBSS. The preferential orientation of Type 1 texture induces liquid spreading in the direction of the LIPSS, leading to lower values of contact angles in this direction. The expressive wetting observed on the Type 4 texture can be explained by the effect of capillarity in the deep valleys between the ridges, which allow expulsing trapped air as the liquid penetrates. The present results show that surface anisotropy plays a crucial role in the wetting behaviour because anisotropic textures (Types 1 and 4) present better wettability than isotropic ones (Types 2 and 3). This hydrophilicity may potentially increase the adsorption and spreading of certain proteins present in the extracellular matrix (ECM), which are responsible for the formation of a framework for cell adhesion. Cell adhesion is significant on all surfaces as shown by the elongated shape of FAPs, which indicates FAPs growth and maturity **[20]**. However, the adhesion strength is lower on the laser nanotextured surfaces, due to the decrease of the FAPs area and by the lower spreading of the cytoskeletons as compared to the smooth control surfaces. At this point, we cannot precisely explain the effect of the surface topography on the differentiation of hMSCs. Further studies are being performed in order to evaluate hMSCs differentiation by assessing the expression of specific osteoblast markers such as osterix (OSX), osteopontin (OPN) and osteocalcin (OCN) and by mineralization assays. However, some possible explanations can be inferred from the cytoskeleton shape, FAPs and cell proliferation, taking into account previous studies. It has been shown that hMSCs commitment and differentiation may be predicted based on the cytoskeleton shape and FAPs formation **[21]**. Osteoblastic lineage commitment is usually verified on cells that spread, generating tension on the F-actin fibers. High actomyosin contractility has been reported as one of the factors responsible for inducing osteogenic differentiation **[22-23]**. The stress on F-actin fibers is transmitted to the FAPs, which tend to elongate in the stress direction. All the surfaces studied in the present work induce different cytoskeleton shapes and different stresses on F-actin fibers, especially LIPSS. This may indicate the possibility of osteoblastic differentiation. Another important aspect concerns the cells proliferative state regarding the differentiation pathway of MSCs. Usually, osteogenesis involves the differentiation of hMSCs into osteoprogenitor cells, pre-osteoblast cells, osteoblasts and osteocytes **[20]**. A high proliferative state is usually verified for osteoprogenitor cells while low proliferative states are commonly observed for osteoblasts. Therefore, the low proliferation observed for the laser nanotextured surfaces can be an indication of a more

advanced differentiation state than for the smooth control surface, where significant proliferation was verified.

Conclusions

The present work shows that ulltrafast laser texturing of Ti-6Al-4V surfaces is an efficient technique for increasing surface wettability and for controlling the behavior of hMSCs. Textured surfaces consisting of LIPSS, nanopillars, and nano-textured microcolumns present an hydrophilic behavior and high affinity for HBSS. Surface texture anisotropy is crucial in controlling the wetting behavior. Cell spreading and adhesion are reduced by laser texturing. Cytoskeleton stretching and stress fibers were clearly observed on LIPSS, while significant filopodia formation was observed on nanopillar textures. No cell proliferation was observed on the laser textured surfaces.

Meet the Authors

Alexandre Cunha is a Ph.D. student in Materials Engineering in the scope of IDS-FunMat-International Doctoral School in Functional Materials for Energy, Information Technology and Health, at Instituto Superior Tecnico (IST), Technical University of Lisbon, Portugal, in a collaboration with University of Bordeaux I, France. He has a Master degree in Materials Engineering and Technology from Pontifical Catholic University of Rio Grande do Sul, Brazil. His research interests include laser surface modification of biomedical grade titanium alloys.

Vitor Oliveira is currently a Professor in the Physics Department of Instituto Superior de Engenharia de Lisboa (ISEL), Portugal. He has a Ph.D. in Materials Engineering. He is also a researcher in the Laser Materials Processing Group of IST. His research interests include laser processing of metals, ceramics and polymers.

Ana Paula Serro is an Associated Professor at Instituto Superior de Ciências da Saúde Egas Moniz (ISCSEM), Portugal. She is also an Assistant Researcher at Centro de Química Estrutural (CQE) at Instituto Superior Tecnico (IST), Technical University of Lisbon, Portugal. She has a PhD in Chemistry. Her research interests include biotribology, biomolecules adsorption onto biomaterials, and biomaterials characterization. Recently, she started a new research line based on drug release from biomaterials.

Omar El-Farouk Zouani is a Post-doc researcher at INSERM, CBMN-UMR 5248, University Bordeaux I, France. He is also a researcher at TEKNIMED Company, L'Union, France, being responsible for the project: "BMPs and Tissue Regeneration". He has a Ph.D. in Biophysics, Applied Biological Sciences and Engineering, University Bordeaux II, France. He is involved in several different international collaborations. He has co-authored about 20 scientific papers in international journals and patents, especially in the fields of Biomaterials, Stem-cell differentiation and Cell mechanics.

Amélia Almeida is an Assistant Professor in the Department of Chemical Engineering of Instituto Superior Tecnico (IST), Technical University of Lisbon, Portugal. She has a Ph.D. in Materials Engineering. She works in LaserMat - Materials Processing and Design Group of IST and has collaborated in several National and European funded research projects. Amelia has authored more than 90 publications in international journals and conferences. Her research interests include laser surface modification of biomedical alloys, laser development of alloys and composites, phase transformations, structural, wear and mechanical characterization of materials.

Marie-Christine Durrieu is a researcher at INSERM, CBMN-UMR 5248, University Bordeaux I, France. She was the Research Coordinator in Biofunctional Surface Engineering at INSERM U1026 BioTis. Recently, she joined Reiko Oda's group in CBMN. Her research interests include surface functionalization, micro-, nano-patterning of materials using peptides for favouring cell adhesion, migration and differentiation.

Rui Vilar is Full Professor in the Department of Chemical Engineering of Instituto Superior Tecnico (IST), Technical University of Lisbon, Portugal. He has a Ph.D. in Physical Metallurgy at University of Paris Sud, Orsay, France. He is the head of LaserMat - Materials Processing and Design Group of IST and of the IST's Platform in Materials and Nanotechnology. Rui has been involved and coordinated a significant number of national and international research projects. He has been working in industrial applications of lasers and laser materials processing since 1987 and has authored more than 450 scientific publications in international journals and conference proceedings.

Acknowledgements

Alexandre Cunha acknowledges the Fundação para a Ciência e a Tecnologia (FCT) for the doctoral grant SFRH/BD/61002/2009. The authors also acknowledge the Programme d'Actions Universitaires Intégrées Luso-Françaises (PAUILF) for financial support in the scope of the International Doctorate School in Functional Materials for Energy, Information Technology and Health (IDS-FunMat).

References

[1] Romanov, Y.A., Svintsitskaya, V.A., Smirnov, V.N. (2003) Searching for Alternative Sources of Postnatal Human Mesenchymal Stem Cells: Candidate MSC-Like Cells from Umbilical Cord, Stem Cells 21, 105-110.

[2] Ohlstein, B., Kai, T., Decotto, E., Spradling, A. (2004) The stem cell niche: theme and variations, Current Opinion in Cell Biology 16, 993-699.

[3] Webster, T.J., Ahn, E.S. (2007) Nanostructured biomaterials for tissue engineering bone, Advances in Biochemical Engineering / Biotechnology 103, 275-308.

[4] Anselme, K. (2000) Osteoblast adhesion on biomaterials, Biomaterials 21, 667-681.

[5] Anselme, K., et al. (2010) The interaction of cells and bacteria with surfaces structured at the nanometre scale, Acta Biomaterialia 6, 3824-3846.

[6] Park, J., Bauer, S., Von der Mark, K., Schmuki, P. (2007) Nanosize and Vitality: TiO2 nanotube diameter directs cell fate, Nano Letters 7 (6), 1686-1691.

[7] Oh, S., et al. (2009) Stem cell fate dictated solely by altered nanotube dimension, PNAS 106 (7), 2130-2135.

[8] Kilian, K.A., Bugarija, B., Lahn, B.T., Mrksich, M. (2010) Geometric cues for directing the differentiation of mesenchymal stem cells, PNAS 107 (11), 4872-4877.

[9] Das, R.K., Zouani, O.F., Labrugère, C., Oda, R., Durrieu, M.-C. (2013) Influence of Nanohelical Shape and Periodicity on Stem Cell Fate, ACS NANO 7 (4), 3351-61.

[10] Anselme, K., Bigerelle, M. (2006) Modelling approach in cell/material interactions studies, Biomaterials 27, 1187–1199.

[11] Norman, J.J., Desai, T.A. (2006) Methods for Fabrication of Nanoscale Topography for Tissue Engineering Scaffolds, Annals of Biomedical Engineering 34 (1), 89-101.

[12] Engel, E., Martínez, E., Mills, C.A., Funes, M., Planell, J.A., Samitier, J. (2009) Mesenchymal stem cell differentiation on microstructured poly (methyl methacrylate) substrates, Annals of Anatomy 191, 136-144.

[13] Dalby, M.J. (2007) Cellular response to low adhesion nanotopographies, International Journal of Nanomedicine 2 (3), 373-381.

[14] Lei, Y., Zouani, O.F., Rémy, M., Ayela, C., Durrieu, M.-C. (2012) Geometrical Microfeature Cues for Directing Tubulogenesis of Endothelial Cells, Plos One 7, e41163.

[15] Vorobyev, A.Y., Guo, C. (2013) Direct femtosecond laser surface nano/microstructuring and its applications, Laser Photonics Reviews 7 (3), 385-407.

[16] Oliveira, V., Ausset, S., Vilar, R. (2009) Surface micro/nanostructuring of titanium under stationary and non-stationary femtosecond laser irradiation, Applied Surface Science 255, 7556-7560.

[17] Oliveira, V., Cunha, A., Vilar, R. (2010) Multi-scaled femtosecond laser structuring of stationary titanium samples, Journal of Optoelectronics and Advanced Materials 12 (3), 654-658.

[18] Cunha, A., Serro, A.P., Oliveira, V., Almeida, A., Vilar, R., Durrieu, M.-C. (2013) Wetting behaviour of femtosecond laser textured Ti-6Al-4V surfaces, Applied Surface Science 265, 688-696.

[19] Li, D., Neumann, A.W. (1992) Contact angles on hydrophobic solid surfaces and their interpretation, Journal of Colloid and Interface Science 148, 190-200.

[20] Dalby, M.J., Biggs, M.J.P. (2010) Focal adhesion in osteoneogenesis, Proceedings of the Institution of Mechanical Engineers, Part H: Journal of Engineering in Medicine 224 (12), 1441-1453.

[21] Zhang, D., Kilian, K.A. (2013) The effect of mesenchymal stem cell shape on the maintenance of multipotency, Biomaterials 34, 3962-3969.

[22] Mathieu, P.S., Loboa, E.G. (2012) Cytoskeletal and Focal Adhesion Influences on Mesenchymal Stem Cell Shape, Mechanical Properties, and Differentiation

Down Osteogenic, Adipogenic, and Chondrogenic Pathways, Tissue Engineering: Part B 18 (6), 436-444.

[23] McBeath, R., Pirone, D.M., Nelson, C.M., Bhadriraju, K., Chen, C.S. (2004) Cell Shape, Cytoskeletal Tension, and RhoA Regulate Stem Cell Lineage Commitment, Developmental Cell 6, 483-495.